Fluid-solid interaction in arteries incorporating the autoregulation concept in boundary conditions

Damon Afkari and Felipe Gabaldón

ABSTRACT

In pre-surgery decisions in hospital emergency cases, fast and reliable results of the solid and fluid mechanics problems are of great interest to clinicians. In the current investigation, an iterative process based on a pressure-type boundary condition is proposed in order to reduce the computational costs of blood flow simulations in arteries, without losing control of the important clinical parameters. The incorporation of cardiovascular autoregulation, together with the well-known impedance boundary condition, forms the basis of the proposed methodology. With autoregulation, the instabilities associated with conventional pressure-type or impedance boundary conditions are avoided without an excessive increase in computational costs. The general behaviour of pulsatile blood flow in arteries, which is important from the clinical point of view, is well reproduced through this new methodology. In addition, the interaction between the blood and the arterial walls occurs via a modified weak coupling, which makes the simulation more stable and computationally efficient. Based on in vitro experiments, the hyperelastic behaviour of the wall is characterised and modelled. The applications and benefits of the proposed pressure-type boundary condition are shown in a model of an idealised aortic arch with and without an ascending aorta dissection, which is a common cardiovascular disorder.

KEYWORDS

FSI; pressure boundary condition; autoregulation; impedance; aorta

1. Introduction

Computational biomechanics researchers try to gain more confidence and draw the attention of clinicians to their colourful contour plots by improving the reliability of the results and by reducing the computational time of the numerical analyses. Sophisticated numerical methodologies have been developed over the last decade. A wide investigation on carotid geometry, developing realistic boundary conditions and post-processing the blood flow profiles on different common, left and right carotid sections has been carried out in Urquiza et al. (2006). Computational fluid dynamic of abdominal aorta with aneurysm disease is simulated and analysed in detail in Les et al. (2010). The use of realistic geometries has permitted them to evaluate precisely the wall shear stresses in these artery bifurcations. Detailed simulations of blood flow in aortic arch, descending, thoratic and abdominal aorta are carried out by Kim, Figueroa et al. (2009), Kilner et al. (1993), Klipstein et al. (1987), Figueroa, Taylor et al. (2009), Tan et al. (2009), Borghi et al. (2008), Artoli et al. (2006), Papaharilaou et al. (2007) and Taylor et al. (1998). Although highly precise, all these sophisticated simulations demand powerful resources thereby limiting the interest of their techniques for emergency clinical applications in hospitals and operation rooms. In the current investigation, various cardiovascular and numerical aspects are combined to reproduce the measurable clinical parameters, such as the blood pressure and the flow rate in different branches of a simulated arterial region. The objective of the current investigation is to propose a method for obtaining a clinically useful simulation of the pulsatile blood flow in arteries with moderate computational resources. Conventional methodologies, as developed by mathematicians and biomechanical engineers, do simulate in detail the blood flow and arterial wall behaviours, but they are too slow for fast clinical diagnostics or pre-surgery decision-making. The current investigation tries to simplify the parameters that slow down the calculations expensive without losing track of the important clinical parameters such as the flow rate in each arterial branch and the pressures in the studied area. Such parameters are the basis for fast decisions that surgeons may need to make while the patient is under clinical check-ups or in emergency care.

In order to achieve realistic simulations in the cardiovascular system, several issues need to be considered, one of them being the interaction of the arterial walls with the pulsatile blood flow. The effect of non-linear flexible arteries are considered with special interest on investigation of probable dissecting walls in Gao et al. (2009). In most of the computational developments at INRIA (France), the arterial wall-blood flow interaction is incorporated in the investigations. The mathematical background of this issue is detailed in Gerbeau et al. (2005), with applications on a realistic geometry of carotid bifurcation. The effects of Fluid–solid interaction (FSI) issue on arterial wall shear stresses are evaluated in Zhao et al. (2000), while stress in the walls are studied in Scotti et al. (2007), Papaharilaou et al. (2007) and Malvé et al. (2012). In numerical simulations, depending on the objectives of a simulation, different coupling techniques can be adopted. For the reasons described in Section 2.3, a modified weak coupling is chosen here in preference to a strong coupling which entails a higher computational cost.

Simulations that include a large part of the cardiovascular system require computationally expensive calculations; hence, it is common to concentrate the studies on a specific region of interest, such as the aortic arch studied here. To avoid errors in the flow-split at different arterial branches, realistic boundary conditions must be used. The distal and proximal zones of the simulated cardiovascular site must be considered in the boundary conditions because of their effects on the resulting blood flow pattern and arterial wall movements (Vignon-Clementel et al. 2010). The results of the simulations, especially the fluid parameters, are very sensitive to the boundary conditions. Although a pressure boundary condition at outlets is a simple and a well-known method, invasive methods must be used to determine the pressures with the accuracy required for numerical simulations. The results are quite sensitive to the imposed values and even small errors in the synchronization of the measured pressures cause significant deviations in the results. The sensitivity of the results arises because of the relatively high kinetic energy of the blood flow and because the physiological pressure oscillations are far greater than the small pressure drops that occur within the region studied. By incorporating the autoregulation of the cardiovascular system, flow-split errors caused by imposing unrealistic pressures are avoided. In addition, a physiologically realistic pressure and flow distribution is achieved while the impedance boundary condition is essentially satisfied. As a sample application of the proposed method, an idealised geometry of a healthy aortic arch is modelled and the results are compared to those of a similar model with a dissected wall.

Autoregulation is a vital controlling phenomenon in the cardiovascular system that guarantees a constant blood nutrition in each arterial branch and, especially, in distal members. After standing up suddenly, one may feel dizzy or lose eyesight briefly, which is attributed to a pressure drop in the head and brain arteries. The cardiovascular system recovers its normal state by an autoregulation mechanism. The heart starts to beat faster, while the arterioles and capillaries increase their diameter, decreasing the flow resistance and facilitating the flow to the affected sites. Changes in blood pressure are detected by baroreceptors in distal sites and activate regulation mechanisms such as dilation or restriction in smooth muscle cells of the small arteries. If a disorder occurs in a cardiovascular site with several outlets in downstream, the autoregulation mechanism reactivates by a diameter change in small arteries in distal areas and regulates the blood flow distribution in the body, redirecting the flow to the branch where the blood delivery is insufficient (Vlachopoulos & O'Rourke 2000a).

Without a regulatory mechanism, there would be considerable drops in blood flow and supply of nutrients. It is assumed that in normal conditions, the blood demanded by each branch is constant and given by the nutrition needs of distal members depending on their physical or physiological activities. Any disorder in proximal areas, such as an atheroma, haemorrhage or a dissected wall may activate autoregulation mechanisms to achieve the blood flow demanded by the distal members, which is independent of proximal disorders in the cardiovascular system.

As mentioned before, together with the autoregulation concept, an impedance boundary condition is incorporated in the present methodology. The cardiovascular impedance is defined by downstream demand of blood, independently of changes in upstream arteries and proximal arterial conditions (Vlachopoulos & O'Rourke 2000b). The impedance is sometimes referred to as the 'hydraulic load' (Mazzaro et al. 2005). The concept is very attractive for establishing realistic boundary conditions that are representative of the rest of the cardiovascular system (Avolio 1980; Sharp et al. 2000; Malvé et al. 2001; Vignon-Clementel 2006; Kim, Figueroa et al. 2009; Figueroa, Baek et al. 2009).

The impedance is normally defined in the frequency domain, while the flow and pressure values are measured and presented in the time domain. By definition, as described in more detail in Section 2.4, the impedance is calculated as a ratio of the Fourier-transformed values of pressure and flow. The definition and interpretation of the impedance concept in cardiovascular systems is presented in Nicholas and O'Rourke (2005), which clarifies that the impedance at a specific site only depends on the vascular bed beyond it. The arteriole bed controls the downstream resistance and small changes in arteriole bed diameters may alter the resistance considerably. With

many arterioles, the resistance may change drastically even if each arteriole modifies its diameter only slightly. In large arteries, although their diameter changes due to autoregulation, the resistance is barely modified. Thus, the arterial tone and impedance of the large arteries can be considered constant. This is why if a large artery suffers from a disorder, the impedances of the outlets of that site are not modified. Also, it is known that if an artery detects a disorder (such as an occlusion in the blood path), the downstream flow and pressure remain essentially unaltered until the disorder reaches a critical stage (Avolio 1980). Before that, when the artery is almost occluded with the blood still flowing, the autoregulation of the cardiovascular system preserves the values of pressure and average flow, which are the parameters that define the impedance. Hence, the impedance values remain almost constant. It must be added that although the pressure in distal sites drops as a consequence of the disorder, this change is relatively small; in the frequency domain, this translates into a decrease of the impedance values at low frequencies (discussed further in the model presented in Section 3). In cardiovascular sites, the impedance function shows a peak in low and null frequencies, which causes numerical instabilities when applying impedance boundary conditions. The impedance values at higher frequencies remain unchanged, despite the autoregulation reaction of the cardiovascular system. In addition, the impedance of a cardiovascular site remains constant at different heart rates (Nicholas & O'Rourke 2005).

In cardiovascular simulations, the impedance boundary conditions are known to improve the modelling accuracy with respect to that achieved with pressure-imposed boundary conditions (Olufsen 1998; Calvo 2006; Vignon-Clementel 2006). In these references, the conventional implementation of the impedance boundary condition requires incorporating the impedance inside the fluid dynamics equations, which increases the computational cost. By contrast, in the proposed methodology, the impedance calculation is separated from the fluid domain equations: the impedance calculations are performed at the end of each cardiac cycle, when new boundary conditions are obtained for the next cycle. This strategy avoids added costs when incorporating the impedance boundary condition (refer to Section 2.4 for more details).

Following a detailed discussion of the boundary condition proposed, the methodology used for fluid, solid and FSI calculations is described in Section 2. In Section 3, the methodology is evaluated using an idealised geometry of a healthy aorta and one with a dissection disorder is described and discussed. While the healthy case serves as a reference simulation, the dissected aorta model challenges the proposed boundary condition when the arterial site suffers from a severe disorder. The limitations of the proposed methodology are discussed in Section 3.3 and the conclusions appear in Section 4.

2. Methodology

The numerical and technical issues corresponding to the simulation methods applied in this work are explained in the current section. The fluid, solid and FSI aspects are discussed first, after which the fluid outlet boundary condition is described in detail.

2.1. Computational fluid dynamics

Blood is treated as an incompressible Newtonian fluid and for healthy arteries, the fluid regime is known to be laminar, though a disorder may change the local regime to turbulent (Vlachopoulos & O'Rourke 2000a; Nicholas & O'Rourke 2005). In the current research, the pulsatile blood flow becomes turbulent due to the dissected flap of the arterial wall (see Section 3.2), which disturbs the blood flow in the ascending aorta. To capture the local turbulence, the Spalart–Allmaras turbulence model has been adopted in this work.

The fluid movement is defined by the Navier–Stokes equations, which are formulated with an Arbitrary-Lagrange-Euler (ALE) scheme. Due to wall deformation, the fluid–solid interface is not fixed. Let $\Omega_f(t) \in \mathbb{R}^3$ be the fluid domain, let $\Gamma_v(t)$ and $\Gamma_t(t)$ be the boundaries of $\Omega_f(t)$ with imposed movements and tractions, respectively, while $\Gamma_v(t) \cup \Gamma_t(t) = \Omega_f(t)$ and $\Gamma_v(t) \cap \Gamma_t(t) = \emptyset$. Besides, $\Sigma(t)$ is the boundary of $\Omega_f(t)$ which is in contact with the arterial wall and $\boldsymbol{n}^{\mathrm{f}}$ is the outward normal vector of the points of $\Gamma_t(t)$.

The ALE formulation of the laminar blood flow problem is defined with the following equations:

$$\rho_f\left(\frac{\partial \boldsymbol{v}}{\partial t} + \boldsymbol{c}\cdot\boldsymbol{\nabla}\boldsymbol{v}\right) + \boldsymbol{\nabla}p - 2\mu\boldsymbol{\nabla}\cdot\boldsymbol{D} = \boldsymbol{0} \quad \text{in } \Omega_f(t) \tag{1}$$

$$\boldsymbol{\nabla}\cdot\boldsymbol{v} = 0 \quad \text{in } \Omega_f(t) \tag{2}$$

$$\boldsymbol{v} = \bar{\boldsymbol{v}} \quad \text{in } \Gamma_v(t) \tag{3}$$

$$\boldsymbol{\sigma}^{\mathrm{f}}\cdot\boldsymbol{n}^{\mathrm{f}} = \bar{\boldsymbol{t}}^{\mathrm{f}} \quad \text{in } \Gamma_t(t) \tag{4}$$

$$\boldsymbol{v} = \boldsymbol{v}_0 \quad \text{in } \Omega_f(0) \tag{5}$$

being the blood flow $\boldsymbol{v}$ and the pressure p the unknowns of the problem. It must be added that the body forces have

been neglected, and $\boldsymbol{c} = \boldsymbol{v} - \dot{\Omega}(t)$ is the relative velocity of the fluid with respect to the velocity of the fluid domain. $\boldsymbol{\nabla}$ and $\boldsymbol{\nabla}\cdot$ are the gradient and divergence operators, respectively. $\boldsymbol{D}$ is the symmetric part of the velocity gradient, ρ_f and μ are the density and the viscosity of blood, respectively. $\boldsymbol{\sigma}^{\mathrm{f}}$ is the Cauchy stress tensor at fluid points.

The Equation (1) corresponds to the balance of linear moment, while (2) is the incompressibility equation, and (3) and (4) are the boundary conditions (with $\overline{\boldsymbol{v}}$ imposed velocities and $\overline{\boldsymbol{t}}^{\mathrm{f}}$ imposed tractions). The Equation (5) are the initial conditions (verifying $\boldsymbol{\nabla}\cdot\boldsymbol{v}_0 = 0$).

The standard boundary conditions defined in (4) will be introduced in terms of imposed pressure histories computed from the cardiovascular impedance of each outlet, as described in Section 2.4.

The weak form of Equations (1), (2), (3) and (4) is discretised and solved using the finite volume method implemented in the commercial CFD programme STAR-CCM+ (CD-adapco 2012). This software employs a polyhedral discretisation which tends to be more accurate than those based on tetrahedral or hexahedral elements (Brezzi et al. 2005).

2.2. Computational solid mechanics

The arterial wall is considered to be an isotropic incompressible hyperelastic material, with a deformed configuration denoted by $\Omega_s(t) \in \mathbb{R}^3$. The model of the arterial wall is established in the framework of continuum solid mechanics, with a Lagrangian formulation in which the movement of $\Omega_s(t)$ coincides with that of the solid particles.

Let $\partial_u\Omega_s(t)$ and $\partial_t\Omega_s(t)$ be the boundaries of $\Omega_s(t)$ with imposed displacements and tractions, respectively, ($\partial_u\Omega_s(t) \cup \partial_t\Omega_s(t) = \Omega_s(t)$ and $\partial_u\Omega_s(t) \cap \partial_t\Omega_s(t) = \emptyset$). In addition, $\Sigma(t)$ is the part of the boundary of $\Omega_s(t)$ which is in contact with the fluid domain $\Omega_f(t)$. Furthermore, $\boldsymbol{n}^{\mathrm{s}}$ is the outward normal vector to the points of $\partial_t\Omega_s(t)$.

The formulation of the problem for the arterial wall is established with the following equations:

$$\boldsymbol{\nabla}\cdot\boldsymbol{\sigma}^{\mathrm{s}} = \rho_s\ddot{\boldsymbol{u}} \quad \text{in } \Omega_s(t) \tag{6}$$

$$\boldsymbol{u} = \overline{\boldsymbol{u}} \quad \text{in } \partial_u\Omega_s(t) \tag{7}$$

$$\boldsymbol{\sigma}^{\mathrm{s}}\cdot\boldsymbol{n}^{\mathrm{s}} = \overline{\boldsymbol{t}}^{\mathrm{s}} \quad \text{in } \partial_t\Omega_s(t) \tag{8}$$

$$\boldsymbol{u} = \boldsymbol{u}_0 \quad \text{in } \Omega_s(0) \tag{9}$$

$$\dot{\boldsymbol{u}} = \dot{\boldsymbol{u}}_0 \quad \text{in } \Omega_s(0) \tag{10}$$

being ρ_s the density and $\boldsymbol{\sigma}^{\mathrm{s}}$ the Cauchy stress tensor in the arterial wall points. In these equations, the volumetric forces are neglected and the unknown is the displacement field, $\boldsymbol{u}$.

The weak form of these equations is discretised using a hybrid finite element formulation (Brezzi & Fortin 1991). The corresponding simulation is carried out with Abaqus (SIMULIA 2000). The constitutive model used for the arterial wall is an isotropic hyperelastic Demiray model (Demiray 1972), defined by the internal energy density function W:

$$W = \frac{a}{b}\left[\exp\left(\frac{b}{2}(I_1 - 3)\right) - 1\right] \tag{11}$$

where I_1 is the trace of $\boldsymbol{C}$, the right Cauchy-Green tensor. Besides, a and b are constitutive constants, being a the slope at the origin of the curve of the Cauchy stress-strain uniaxial tensile test. This constitutive model has been implemented in Abaqus via an 'user material' subroutine. The constitutive parameters have been calibrated with experimental in vitro tests conducted at the Material Science Department of the Polytechnical University of Madrid (García-Herrera 2008).

In the current investigation, an isotropic hyperelastic model is implemented. As discussed in Section 2.4, the methodology is based on a staggered interaction scheme and the fluid and solid programmes operate separately. This allows incorporating realistic properties in both domains, such as anisotropic hyperelasticity or viscoelasticty in the walls or non-Newtonian characteristics in the blood. If the simulation concentrates on the solid domain (e.g. stress values in the plaques and walls, fatigue or remodelling effects), a more realistic constitutive model is necessary. With the procedure adopted, any constitutive model can be incorporated for simulating the solid behaviour.

2.3. Fluid–solid interaction

The forces exchanged between the arterial walls and the pulsatile blood flow should be evaluated with special care in cardiovascular simulations; fluid pressures affect the arterial wall movements and the wall deformations influence the blood flow patterns.

The blood flow and wall shear interaction is defined with the following transmission conditions, defined in $\Sigma(t)$:

$$\boldsymbol{v}(t) = \dot{\boldsymbol{u}}(t) \tag{12}$$

$$\boldsymbol{\sigma}^{\mathrm{f}}\cdot\boldsymbol{n}^{\mathrm{f}} + \boldsymbol{\sigma}^{\mathrm{s}}\cdot\boldsymbol{n}^{\mathrm{s}} = \boldsymbol{0} \tag{13}$$

From a computational point of view, there are several procedures for solving Equations (12) and (13) in a discrete manner. The monolithic methods solve simultaneously

the fluid, solid and interaction equations. Although these methods are unconditionally stable, they are computationally expensive because of the nonlinearities of the fluid and solid equations. By contrast, staggered methods solve the fluid and solid problems separately, exchanging the necessary information across their interaction interface. There are staggered methods with implicit (or strong) and explicit (or weak) coupling. The method is called implicit if more than one iteration is required during the data exchange (12), (13).

Although somewhat less precise, an explicit FSI scheme is faster than an implicit coupling. This lack of precision, however, only affects parameters that are clinically less important (such as pulse transmission/reflection, arterial wall velocities, etc.). On the other hand, an explicit FSI coupling may show numerical instabilities when the densities of the two domains are relatively similar (Burman & Fernández 2009), as occurs between densities of the blood and arterial walls. Although an explicit coupling is adopted here, this problem is avoided by applying a modification in the conventional explicit coupling method. The modification consists in neglecting the wall velocities during the data exchange process. This simplification has little effects because the blood velocity is about two orders of magnitude greater than the arterial wall velocity (longitudinal velocity of the blood vs radial velocity of the walls), an observation that has been verified by the authors in several models studied with implicit and modified explicit FSI (Afkari et al. 2014). In this reference, the wall deformations in explicit and implicit FSI methodologies are compared when the cardiac cycle is at its maximum flow rate, and consequently the maximum differences are expected. In addition, the resulting wall shear stress (as the more critical parameter in the formation of arterial plaques and damages) confirms a negligible difference between the two coupling strategies. It is worth mentioning that from the computational point of view, an implicit FSI strategy is about 15 times more time-consuming than an explicit alternative. This factor corresponds to a pulsatile blood flow simulation in a straight artery, and may increase for larger models with more geometrical details and disorders.

The staggered explicit FSI methodology adopted for coupling the codes Abaqus and STAR-CCM+ is managed by the Co-simulation SIMULIA Engine, which manages the data exchange (SIMULIA 2000).

2.4. Proposed boundary condition method

A new method is proposed for applying the boundary conditions at the outlets of a CFD model of the arteries. The Autoregulation & Impedance Pressure Boundary Condition (A+IPBC) method incorporates the autoregulation and impedance concepts both into the classical pressure-imposed boundary condition. An in-house code, written in GNU Octave and AWK, calculates the pressure-imposed values at outlet boundary conditions, which is discussed in detail in the current section. The code is coupled to the CFD programme during the A+IPBC iterations.

Figure 1 shows the details of the steps in the A+IPBC method. This flowchart is applicable for any cardiovascular site at which the flow distribution between outlets is to be calculated. As a sample for application of the method, a dissected aortic arch has been chosen as the one to be investigated (Section 3). The method is of major interest when simulating abnormally deformed or disordered arterial geometries, specially with more than one outlet being the percentage of flow distribution in each outlet as the demanded unknown parameter. The application of the method shows the importance of the flow-split calculations in such geometries and their close correlation with the applied boundary conditions. Through several iterations in the A+IPBC method, a series of appropriate pressure boundary histories (equal to the number of outlets) will be calculated considering the autoregulation and impedance requirements.

In the A+IPBC method, the pulsatile blood flow is known as an inlet boundary condition while the flow and pressure histories at the outlets are unknown. The flow percentages that exit by each outlet, and impedance values at the outlets are also the input data feeding the A+IPBC method. These values are supposed to be individual-dependent constant in healthy adults and in those with a disorder in proximal sites, as it is mentioned in several references such as Vignon-Clementel (2006), Malvé et al. (2001), Avolio (1980), Figueroa, Baek et al. (2009) and Kim, Figueroa et al. (2009). In the proposed methodology, based on the cardiovascular autoregulation concept, the iterations are terminated when the flow-split requirement is satisfied, and therefore, each outlet receives the cardiac pulse-average flow percentages imposed at the start of the A+IPBC procedure. The steps shown in Figure 1 are described as follows:

- Point 1. A CFD model of the studied geometry is run for one cardiac cycle, applying the pulsatile flow at the inlet and a constant mean arterial pressure (MAP) at all outlets to initialise the calculations. An 80 mmHg constant pressure, chosen as the minimum physiological pressure in healthy adults, is suggested to be appropriate for starting the iterations. During the next iterations, this constant pressure-imposed boundary condition will be modified to pulsatile pressure histories, based on the impedance calculations.
- Point 2. Post-processing the CFD results of the point 1, the outlet flows $\{Q_i\}$ are extracted ($i = 1, 2, ...,$ number of outlets).

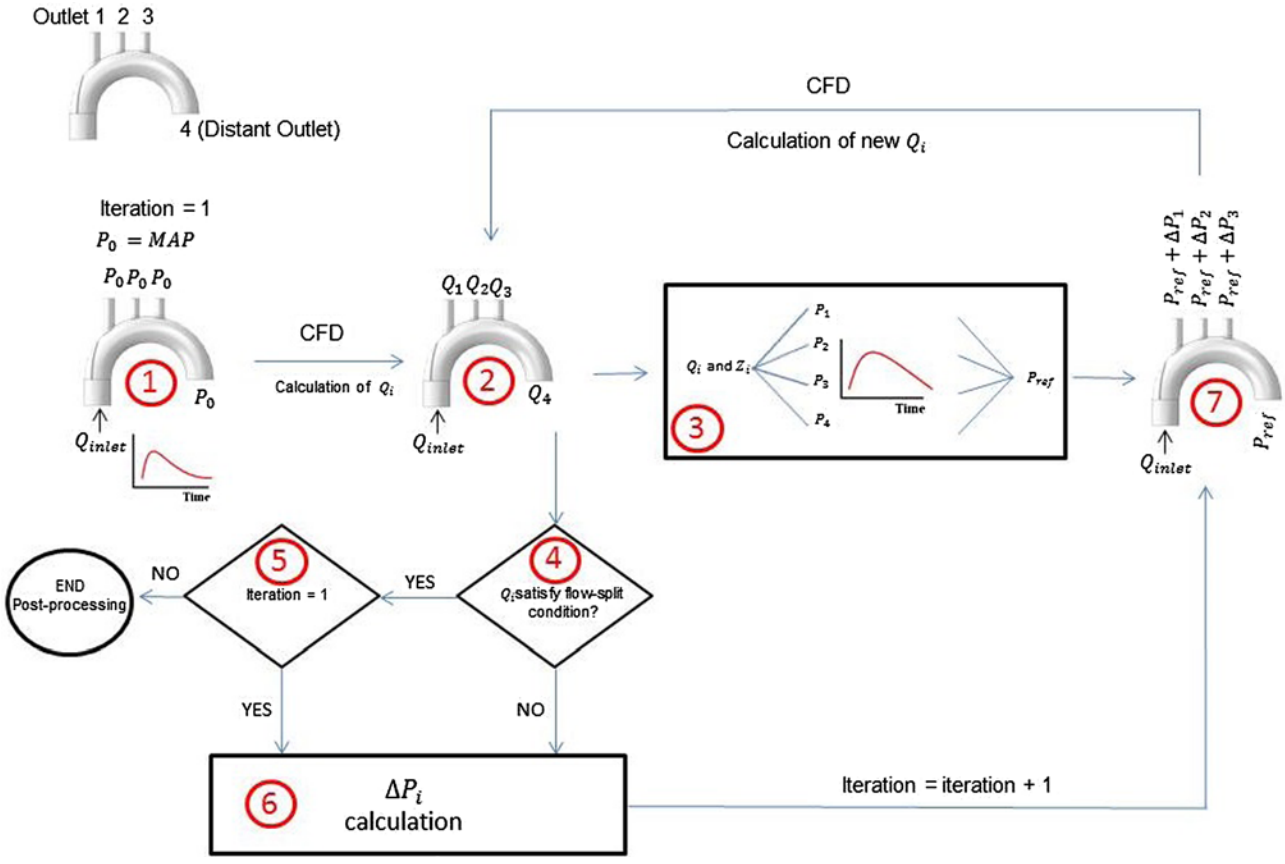

Figure 1. Flowchart of A+IPBC method.

- Point 3. As mentioned before, an in-house code was developed by the authors in order to calculate the new $\{P_i\}$ based on the $\{Q_i\}$ resulted in each cardiac cycle (In a model with 4 outlets, $\{P_i\}$ is four series of pressure histories for four outlets). In this calculation, the Fourier theory is applied. Using Fourier analysis, any periodic function can be decomposed into a sum of harmonic functions. Because in clinical measurements the pressure and flow data are in discrete format, the Fourier transform must be discrete as well. The Discrete Fourier Transform (DFT) and its inverse (IDFT) are defined as follows:
DFT:

$$\hat{X}_j = \frac{1}{N}\sum_{k=0}^{N-1} X_k e^{\frac{-2\pi i}{N}jk}, j = 0, \cdots, N-1 \qquad (14)$$

IDFT:

$$X_j = \frac{1}{N}\sum_{k=0}^{N-1} \hat{X}_k e^{\frac{2\pi i}{N}jk}, j = 0, \cdots, N-1 \qquad (15)$$

where $\hat{X}_j$ are discrete values in the frequency domain and X_j are discrete values in the time domain. N is the number of discrete values, depending on how many data are registered during measuring process. Considering $\{p_j\}$ and $\{q_j\}$ two series of discrete values of pressure and flow in the time domain during one cardiac cycle, while $\{\hat{p}_j\}$ and $\{\hat{q}_j\}$ are their corresponding discrete values in the frequency domain, the impedance for the discrete data is by definition:

$$\hat{z}_j = \frac{\hat{p}_j}{\hat{q}_j} \qquad (16)$$

Considering the expressions of the Discrete Fourier Transform and its inverse, the following result is obtained:

$$\hat{p}_j = \hat{z}_j \hat{q}_j = \hat{z}_j \frac{1}{N}\sum_{k=0}^{N-1} q_k e^{\frac{-2\pi i}{N}jk} \qquad (17)$$

and by direct hand calculations the following result is obtained:

$$p_j = \frac{1}{N}\sum_{k=0}^{N-1} q_k z_{j-k} \qquad (18)$$

Hence, the pressure is expressed in terms of flow and impedance which are both in the time domain.

Equation (18) is implemented in this point of the A+IPBC flowchart. Based on the $\{Q_i\}$ resulted in point 2 of the flowchart, and considering the impedance values which are known at each outlet, the pressure curves $\{P_i\}$ and their instantaneous average value (P_{ref}) are calculated (as it mentioned before, each P_i is a series of p_j values). The P_{ref}, such as $\{P_i\}$, is a pressure-history function of time. The averaging strategy is adopted to avoid possible source of instabilities in the A+IPBC calculations, which may occur at early cardiac cycles if the flow histories differ considerably from the physiological flow values. Therefore, during the A+IPBC iterations the pressure and flow curves are being modified at the end of each iteration based on the impedance values used as input data in the analysis. In each individual, the impedance values of each outlet ($\{z_i\}$) are supposed to be known prior to starting the iterations. In the application of the proposed method in aortic arch discussed in Section 3, these values correspond to the impedances of a healthy adult.

- Points 4 and 5. In parallel to the calculations at point 3, if the flows satisfy the flow-split requirements, and in addition, the A+IPBC procedure is not at its first iteration, the A+IPBC iterations will stop. The procedure should not end in the first iteration because in this iteration, a constant MAP is being applied at the outlets and this is not physiologically correct pressure value; the pressures are actually pulsatile and the A+IPBC method should pass at least once through the impedance calculations (point 3). Hence, although the applied pressure is unrealistic in the first iteration, but in subsequent iterations a physiologically ranged pressure curve is reproduced and imposed at each outlet as a result of the impedance calculations. It is worth mentioning that the application of a reasonable and physiological MAP values at the first iteration is of a greater importance in FSI simulations than when using a CFD model with rigid walls. This is due to the fact that in FSI simulations, an unrealistic pressure at the outlets produces considerable errors in arterial wall dilation, which in turn would affect considerably on the flow-split results. In addition, the unrealistic dilation may also cause instabilities in the CSM simulation.
- Point 6. In this step, a series of pressure difference values are to be calculated in order to be added to the pressure reference value gained at point 3. The proposed pressure series would adjust the pressure-imposed boundary conditions in order to fulfil the flow-split requirement in the next iteration. The pressure differences $\{\Delta P_i\}$ are calculated with respect to the 'distant outlet', which is the one not very affected by the disorder. In each iteration, the procedure passes once through the ΔP_i calculation box. In this box, according to the history of calculated $\{\Delta P_i\}$ during the previous cycles, and their corresponding flow-split at point 2, new $\{\Delta P_i\}$ are determined. It must be added that, i in $\{\Delta P_i\}$, is from 1 to 3 in the sample aortic arch model in which 4 outlets exist; in this model, the 'distant outlet' is the outlet 4 and therefore the ΔP_4 is zero. The A+IPBC method can be applied in simulation of cardiovascular sites with different outlets. In pressure difference calculation box, a least square method is adopted for calculating the new $\{\Delta P_i\}$ values. As it is mentioned above, the new set of $\{\Delta P_i\}$ should be estimated in a way that it reduces the flow-split errors calculated by the next iterations. Considering a graph with the horizontal axis representing the applied pressure difference of each outlet, and the vertical axis as the resulted flow-splits, the history of the applied pressures and their corresponding flow-splits are a set of points which participate in the least square pressure-adjusting procedure. In this methodology, each new point corresponding to the last iteration results will adjust the least-square-fitted lines until they converge to an almost constant line in consecutive iterations. The last fitted-line permits to obtain the final applied pressure difference series with which the flow-split requirement is fulfilled. It is worth emphasising that in each iteration, the calculated $\{\Delta P_i\}$ values are added or subtracted to P_{ref} curve (positive or negative $\{\Delta P_i\}$), depending on if less or more flow is expected to be passed through that outlet. Therefore, in the A+IPBC method, the effects of the autoregulation which is a physical phenomenon (distal arterial dilation or constriction) are incorporated in the boundary conditions by adjusting the imposed pressures at the outlets.
- Point 7: The results of points 3 and 6 are applied again in a CFD model of the same geometry (applying $\{P_i\} + \{\Delta P_i\}$ on each outlet, except the distant outlet on which P_{ref} is applied). The resulting $\{Q_i\}$ would be fed back to point 2. The procedure continues until the flow-split requirements are satisfied.The A+IPBC method is a pressure-imposed boundary condition methodology that can be applied in simulations with rigid or elastic walls. The results of simulation of healthy arteries show that the flow-split is not affected if the walls are considered as rigid or deformable. This is basically due to a relatively small wall deformation during the cardiac cycle, comparing to the general dimensions of the studied area (refer to Section 3.1 for more details). On the contrary, when the arterial site suffers from a severe

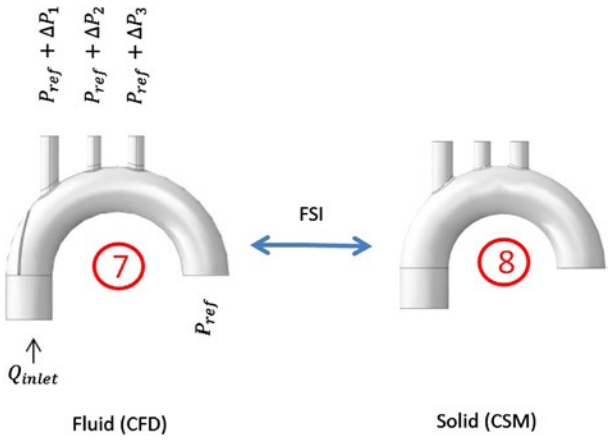

Figure 2. Incorporation of FSI in A+IPBC flowchart.

deformation (e.g. dissection), a rigid assumption of the walls may result in unrealistic analysis. But independently to a healthy or diseased situations of the simulation, a rigid assumption of the arterial walls causes the simulation to lose some results such as pressure pulse transmission or the corresponding results of the solid mechanics field (e.g. stress). It must be emphasised that the adopted simulation strategy (flexible or rigid walls) is independent to the A+IPBC. Referring back to the flowchart, if FSI is to be considered, the only modification in the A+IPBC method concerns the path from point 7 to point 2, while the rest of the flowchart remains unchanged. At this point, the CFD simulation interacts with the CSM model of the arterial walls (Figure 2), via an interaction scheme that follows the coupling strategy explained in Section 2.3. As in the A+IPBC method for rigid walls, after the additional FSI calculations, the simulation time has advanced only one cardiac cycle. Therefore, the extra computational clock-time of the simulation would be attributed to the interaction between CFD and CSM, which in turn, is reduced the most according to Section 2.3 by the modification implemented in the explicit coupling technique.

3. Results and discussion

Based on the geometries of different aortic arches in a number of individuals (Suo 2005; García-Herrera 2008; Qiao & Liu 2008; Votta et al. 2008; Bailevs et al. 2009; Kim, Figueroa et al. 2009; Huang et al. 2010; Moireau et al. 2011; Brown et al. 2012), an idealised geometry shown in Figure 3 is adopted. The studied aortic arch has an internal diameter of 20 mm while the wall thicknesses are 1.2 and 2 mm for the main aortic arch and the uprising outlets, respectively (García-Herrera 2008; Polindara et al. 2013). The A+IPBC method can be applied for different geometries and cardiovascular sites, while the idealised geometry will be used here as a sample on which additional idealised abnormalities can be introduced. Two models will be studied corresponding to a healthy and a dissected aortic arch.

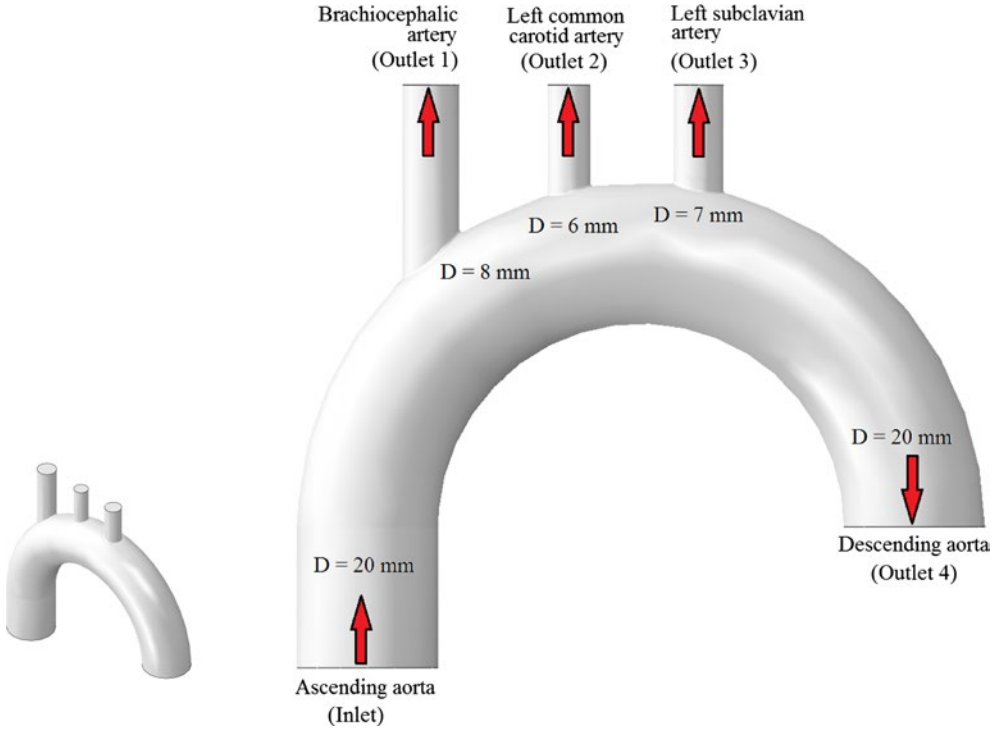

Figure 3. Geometry and dimensions of the simulated aortic arch.

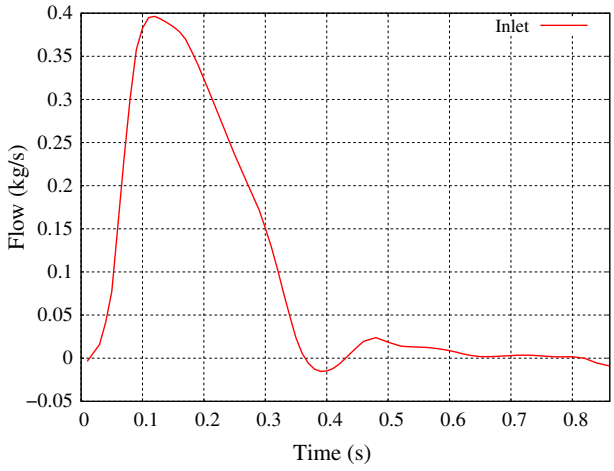

Figure 4. Flow inlet boundary condition at the aortic root Suo (2005).

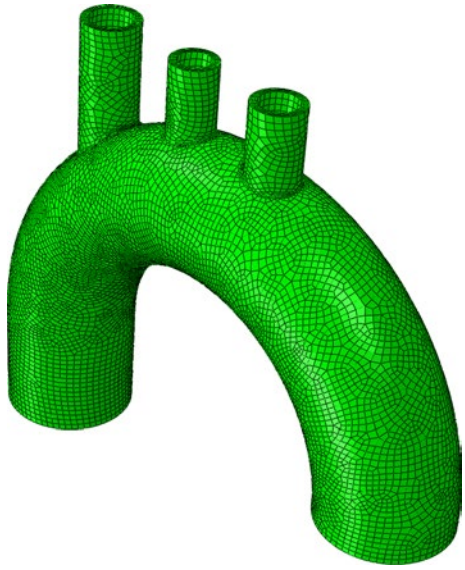

Figure 5. Solid domain of the aortic arch in FSI simulation of a healthy person.

The healthy model will serve as a reference for that with the dissection disorder.

The inlet flow boundary condition for both models corresponds to a healthy male adult based on the values presented in Suo (2005). It is assumed that the heart adjusts its cardiac outlet even if distal cardiovascular sites suffer from a disorder, pumping more potentially in order to satisfy the body's blood demand. Figure 4 shows the mass flow leaving the left ventricle and entering the aortic root. The cardiac cycle is about 860 ms which is a typical heart rate in a healthy adult.

Based on the values mentioned in the references (Shahcheraghi et al. 2002; Suo 2005; Moireau et al. 2011), the time average flow-splits for one complete cardiac cycle are 10, 5, 5 and 80% for the brachiocephalic, left common carotid, subclavian and descending aorta artery, respectively. These values are implemented as input data in all simulations presented in the current section. For other geometries of other cardiovascular sites, one should know these percentages prior to starting the A+IPBC calculations.

As it was mentioned before, the other outlet boundary condition which is incorporated in the calculations is the impedance. The corresponding values are adopted as an average values of outlet impedances in human adult based on different references (O'Rourke & Taylor 1967; Milnor 1975; Avolio 1980; Murgo et al. 1980; Zhao et al. 2000; Nicholas & O'Rourke 2005; Kim, Vignon-Clementel et al. 2009; Vignon-Clementel et al. 2010; Moireau et al. 2011). The values are presented in Figure 11 (Section 3.2), where the converged impedance modulus values are compared to their references in each outlet.

The biomechanical properties of the arteries are based on the values reported in García-Herrera (2008), which are the results of the experimental in vitro tests on several human aortic arch samples. The corresponding parameters of Equation (11) are as follows:

$$a = 54.419kPa, b = 1.936$$

It must be added that in the A+IPBC method, any kind of constitutive model can be implemented for the solid mechanics calculations, but in this work, due to the principal objective which is flow-split evaluations, an isotropic hyperelastic model suffices. The more precise results demanded of the walls, the sophisticated models can be applied.

The solid element discretisation is presented in Figure 5. An eight-node three-dimensional hybrid element (C3D8H) is used in all the simulations. The hybrid formulation is selected in order to avoid the numerical locking caused by the incompressible behaviour of the arterial walls. There are four layers of elements through the thickness, which enables the model to capture deflections very precisely.

All outlet surfaces are free to move in their initial plane position. This is applied by coupling the central point of each outlet to all the nodes lying on the outlet surface. A 'distributing coupling' (SIMULIA 2000) is used for this purpose, with the reference points fixed in space.

Some questions may arise when the solid model is cut at the inlet and outlets, neglecting the effects of the rest of the arterial system and the effect of the heart oscillations. To evaluate this issue, the following items are introduced in the models:

- Added springs representative of the connected arteries: several 5-cm springs are incorporated to the ends of the three uprising arteries and the

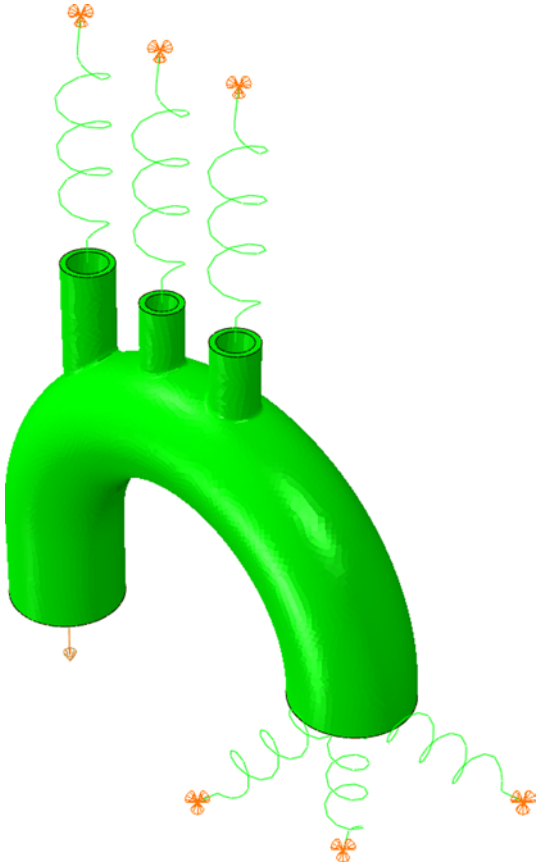

Figure 6. Springs incorporated to represent surrounding tissues.

descending aorta. Figure 6 shows the position and direction of these springs. The springs represent the structural influence of the arteries beyond the outlets, which is not being explicitly modelled. The springs allow the outlets to move around their initial positions in a realistic fashion. In addition, there are two perpendicular springs at the outlet of the descending aorta. They act on the lateral direction and out-of-plane movements, representing the resistance of the surrounding tissues of this specific outlet. The lateral springs are not incorporated in the uprising outlets because no out-of-plane movements are expected there. This is mainly due to their vicinity to the chest or other relatively rigid members.

- Heart movements: The aortic root shows a periodic vertical and rotational oscillation due to the heart movements, being the frequency of the movement that of the heart beat. The movements are imposed in the model according to Beller et al. (2005). A vertical displacement of 8.9 mm and a rotation of about 6 degrees are applied at the central point of the inlet surface coupling. The movements peak at 0.3 s along the cardiac cycle, when the aortic root has displaced and deformed the most by the heart.

Table 1. $\{\Delta P_i\}$ and flow percentages of each outlet during the A+IPBC iterations in FSI simulation of the healthy aortic arch.

	Iter.1	Iter.2	Iter.3	Iter.4
ΔP_1(Pa)	0.0	-5.0	-35.0	-32.3
ΔP_2(Pa)	0.0	-5.0	-40.0	-32.1
ΔP_3(Pa)	0.0	-5.0	-24.0	-26.1
Q_1(%)	6.5	7.0	10.3	9.9
Q_2(%)	2.6	2.9	5.5	4.9
Q_3(%)	2.6	2.1	4.8	5.2
Q_4(%)	88.3	88.0	79.4	80.0

3.1. Healthy aorta

Table 1 lists the successive iterations of the A+IPBC method, converged after four iterations (or cardiac cycles) for the case of the studied healthy aorta. The iterations start with the application of the MAP on all outlets; all $\{\Delta P_i\}$ are equal to zero. In the second loop, a value of -5 Pa is chosen by the in-house code because at the end of the first iteration all flow-splits are lower than the desired ones; 6.5, 2.6 and 2.6% in comparison with 10, 5 and 5%, for the brachiocephalic, left common carotid and subclavian arteries, respectively. Based on the flow-splits of the second iteration, new $\{\Delta P_i\}$ are estimated and used in the third iteration. As this healthy model will serve later as a reference model for comparison with a dissected-wall model, the iterations continue until the flow-splits reach precisely the desired values.

Comparing $\{\Delta P_i\}$ results of the healthy FSI model with the corresponding values in the rigid healthy simulation, the differences are found to be negligible. This is attributed to a relatively small deformation of the elastic walls in a healthy individual. Figure 7 shows the diameter change in all outlets during a cardiac cycle. As can be seen at inlet that deforms the most, the maximum diameter change reaches some 2.5 mm, about 13% change in diameter. The change is smaller at all other outlets, being 8.7% for the case of the outlet 4 or the descending aorta. Such wall deformations change the fluid domain, but are insufficient to modify

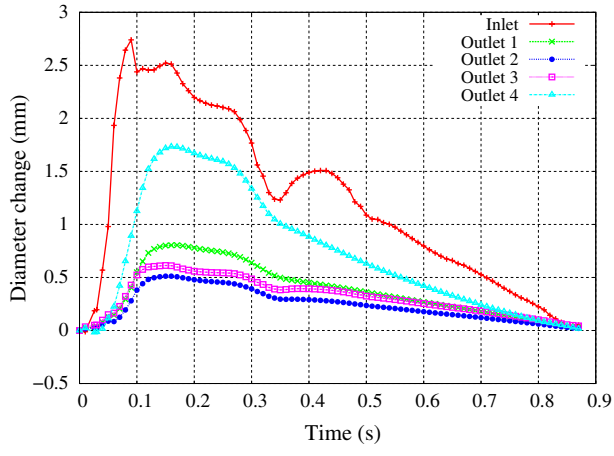

Figure 7. Diameter change of the outlets during one cardiac cycle in FSI healthy model.

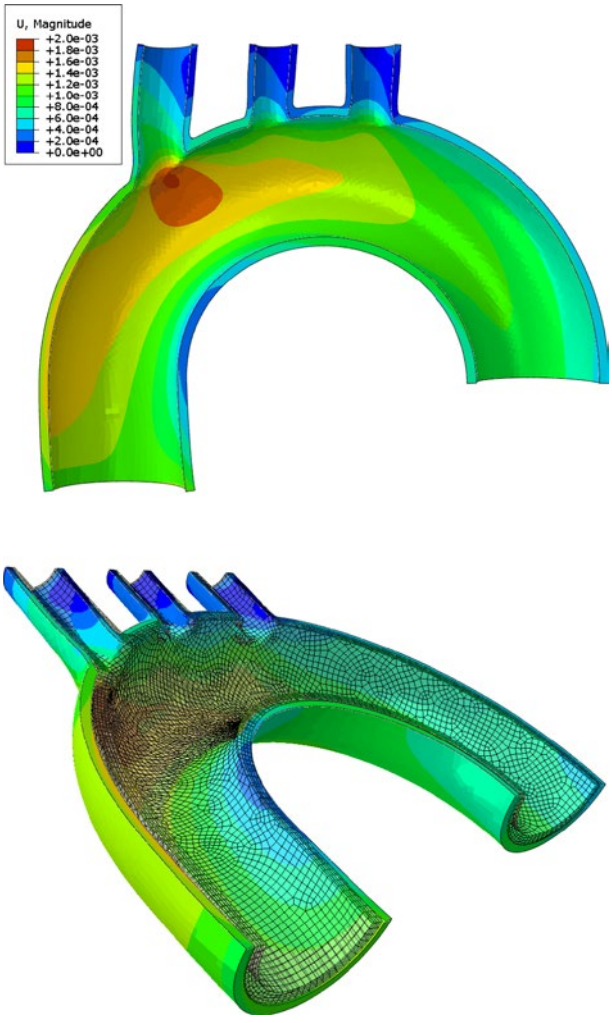

Figure 8. Displacement contours at 0.1s, maximum inlet diameter change (m) (amplified two-fold).

the flow-splits and especially the converged $\{\Delta P_i\}$ values. The section shown in Figure 8 presents the displacements amplified by a factor of 2 for an easier visualisation. In some zones, the maximum displacements arise from the global movement of the aortic body (it should be noted that Figure 7 dealt with diameter changes, not with global movements). Although the dimensions change during the cardiac cycle, the general geometrical shape of the aortic arch maintains and the results coincide with those evaluated with rigid walls. It can be concluded that incorporating FSI in a healthy aortic model has only a minor effect on the flow-split results.

3.2. Dissected aorta

Figure 9 shows the idealised geometry representing a dissection in the inner walls of the ascending aorta. The arterial walls may deteriorate due to aging, smoking or other reasons. Poor structural properties of the arterial wall lead to a dissection in its layers. High blood pressure and congenital deviation in flow patterns may increase the formation risk of this disorder. Continuous entrance of the blood flow to the dissection develops the false lumen sac and severe problems may arise; wall rupture or major disturbances in the blood flow patterns. The latter case is studied in the current section.

In the dissected model, the boundary conditions are the same to those in the healthy model. The structural boundary conditions at the outlets consist in coupling to the reference points, which allow in-plane movements of those sections. For the fluid, the impedances those of the healthy model are implemented. As it discussed in Section , the blood demand is assumed to remain unchanged independently of upstream disorders such as a dissection in the ascending aorta. Therefore, the same impedance values can be used for the dissected model.

Although the dissected part of the wall is assigned by the same properties as those of the walls, its relatively small thickness makes it to behave as a membrane with no bending stiffness. Therefore, its role in the model is to introduce perturbations in the blood flow pattern in order to appraise the stability of the A+IPBC method and

Figure 9. Geometry of the aortic dissection.

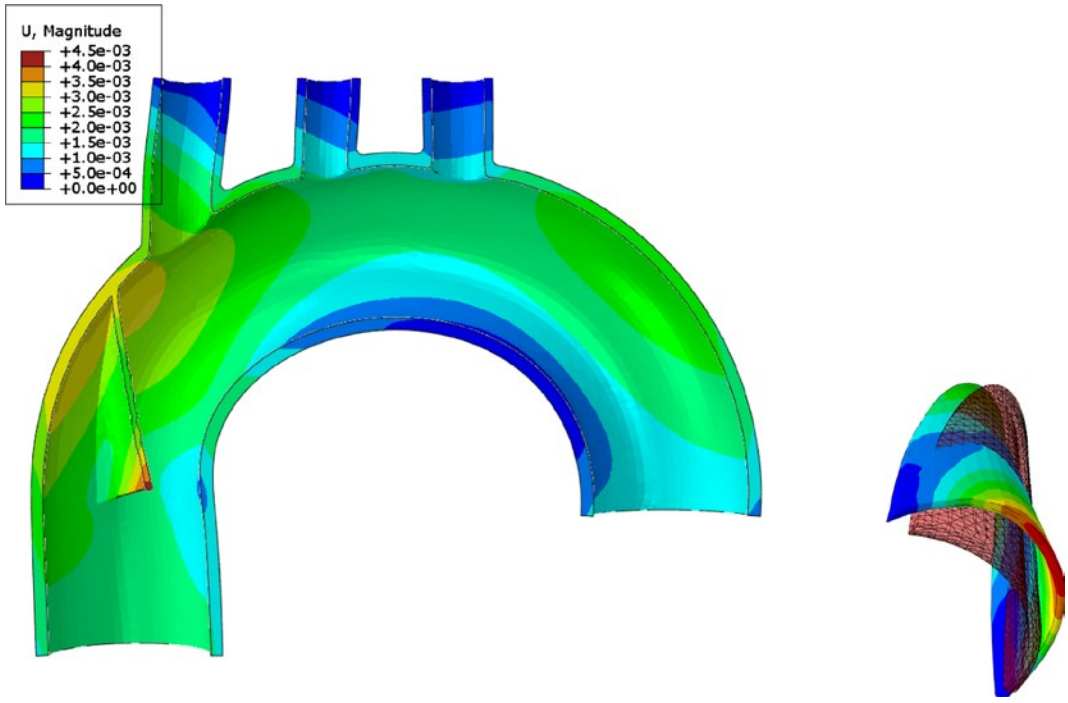

Figure 10. General and zoomed contour view of the maximum deformation of the aortic arch and the dissected layer (m).

Table 2. $\{\Delta P_i\}$ and flow percentages of each outlet during the A+IPBC iterations in the FSI dissected aortic arch.

	Iter.1	Iter.2	Iter.3	Iter.4	Iter.5 (1st cardiac cycle)	Iter.5 (2nd cardiac cycle)
$\Delta P_1(Pa)$	0.0	-150.0	-37.16	-31.40	-30.37	-30.37
$\Delta P_2(Pa)$	0.0	-10.0	-7.25	-18.95	-1.13	-1.13
$\Delta P_3(Pa)$	0.0	-10.0	-6.93	-15.12	-0.66	-0.66
$Q_1(\%)$	4.79	25.82	12.03	10.47	11.14	11.99
$Q_2(\%)$	5.37	4.86	5.84	7.75	5.25	5.35
$Q_3(\%)$	5.34	4.85	5.70	7.45	4.67	4.80
$Q_4(\%)$	84.50	64.47	76.43	74.33	78.94	77.86

evaluating if the convergence is reached in severe-disordered models.

Figure 10 indicates the displacement contours of the complete aortic arch (and specially the detached wall) superimposed on the initial undeformed geometry. The maximum displacement of the tip of the dissected layer reaches 4.5 mm when the blood flow reaches its maximum velocity. It must be emphasised that this value of maximum displacement corresponds to this specific idealised model; hence, in different patients this value may be modified.

Table 2 lists $\{\Delta P_i\}$ values during five iterations before the flow-split values are stabilised. The iterations start without pressure differences with respect to the outlet 4 (zero values of $\{\Delta P_i\}$ in the first column of the table). After the first iteration, the resulting flow-splits differ considerably from the desired values, especially for outlet 1 (the brachiocephalic artery). The process continues until iteration 5. As a general rule, when the flow-split differences are less than 2% in comparison with the desired values, the A+IPBC iterations will be terminated (Iter.5, 1st cardiac cycle). An additional iteration (Iter.5, 2nd cycle) is performed without modifying the last $\{\Delta P_i\}$ values (-30.37 , -1.13 and -0.66 Pa for outlets 1–3, respectively). This additional iteration is realised in order to allow the flow patterns stabilising after two consecutive changes in $\{\Delta P_i\}$ values during the last two iterations (referring to column Iter.4 and Iter.5, 1st cycle). When the simulated site suffers from a disorder, it takes at least two cardiac cycles to the flow-split percentages to be stabilised. But the additional A+IPBC iteration is faster in comparison with a complete A+IPBC iteration because only the path between point 7 and point 2 is repeated (refer back to Figure 1). As seen in the last column (Iter.5, 2nd cycle), the flow-splits have changed with respect to the penultimate column (Iter.5, 1st cycle), while the $\{\Delta P_i\}$ values remain constant.

During the A+IPBC method, adding $\{\Delta P_i\}$ values to P_{ref} may result in a difference between the applied impedance boundary condition and the resulted impedance values calculated based on the last iteration of flow and pressure histories. In order to evaluate the effect of the point 6 of Figure 1 on the converged impedances, Figure 11 compares these values for all aortic arch outlets. As it can be seen, the resulted impedances are satisfactorily similar to the reference impedances (the ones with which the calculations start), while there is a negligible difference

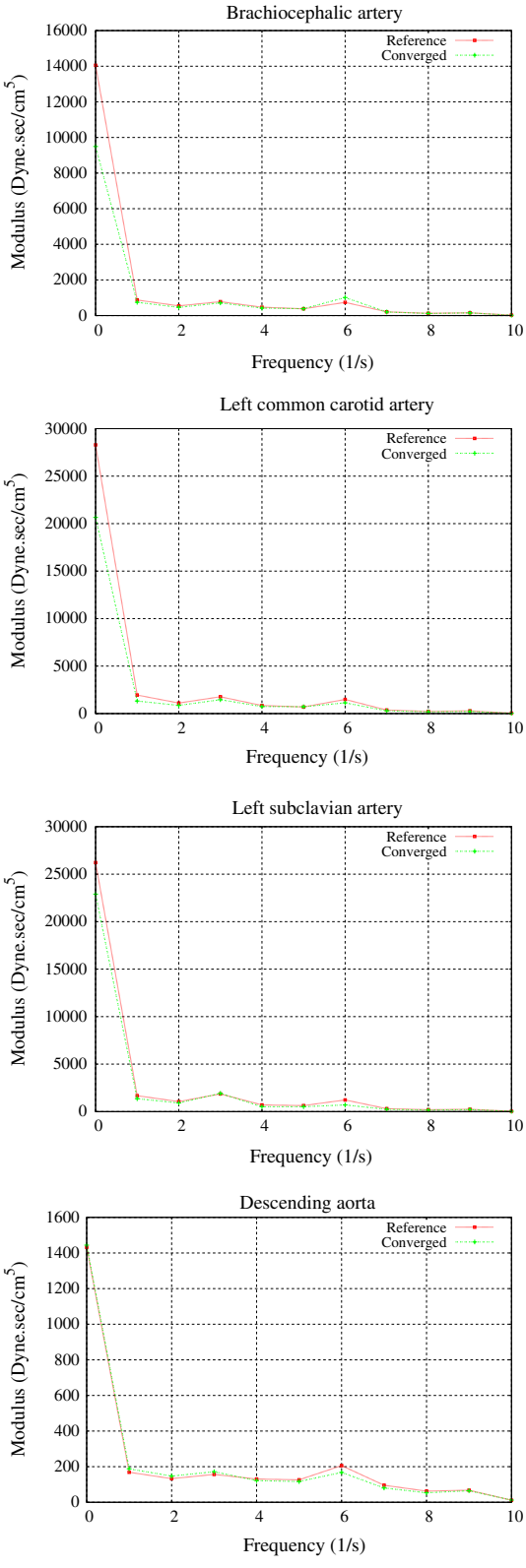

Figure 11. Comparison of modulus values of the reference and the impedances resulted by A+IPBC method.

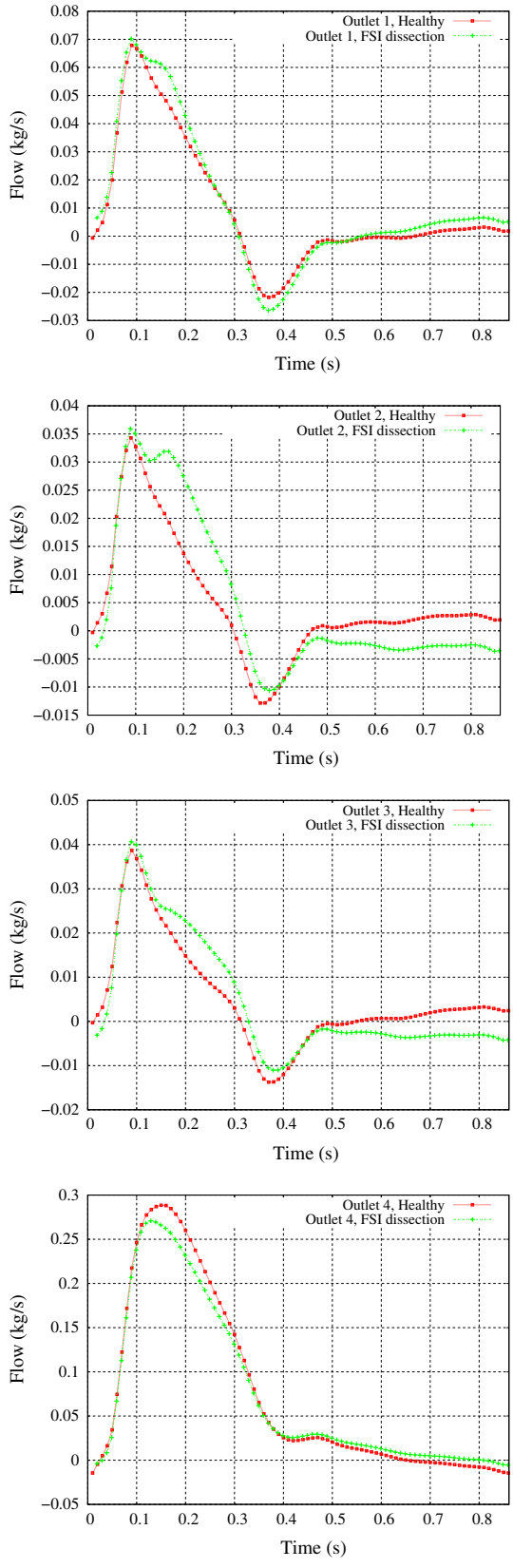

Figure 12. Comparison of mass flow histories in the FSI healthy and dissected aortic arch models (All outlets).

at zero frequency (steady-state mode). This is attributed to adding the constant values of $\{\Delta P_i\}$ (which are small comparing to $\{P_i\}$) to P_{ref}, and in addition, the averaging of $\{P_i\}$ in order to calculate P_{ref}. Therefore, the autoregulation requirements are fulfilled while the reference impedances are implemented in the analysis.

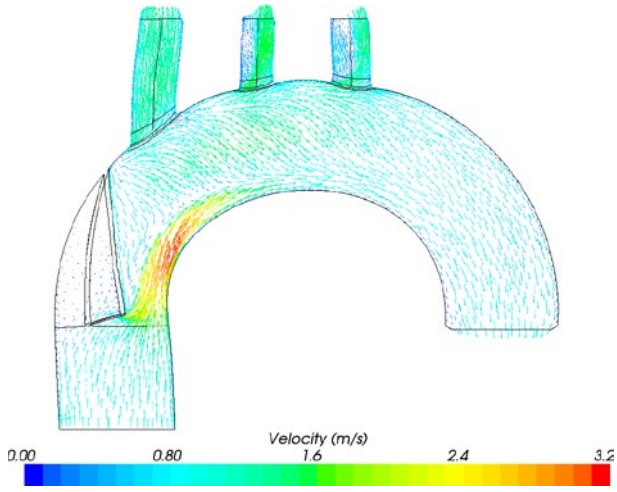

Figure 13. Velocity vectors on a longitudinal cross section at 0.15 s of cardiac cycle of the dissection model.

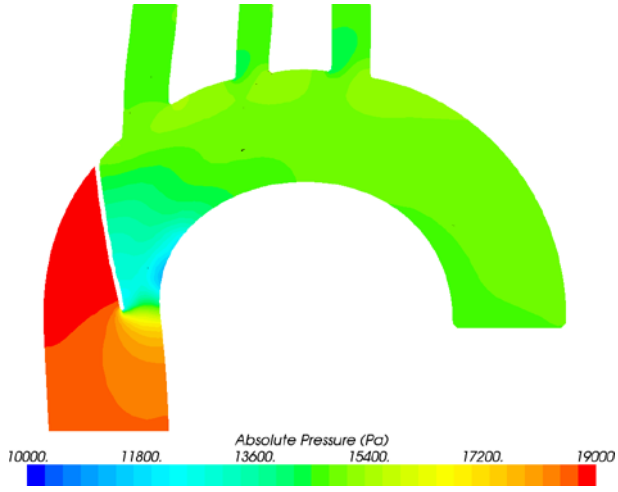

Figure 15. Pressure contour on the longitudinal cross section of the dissection model.

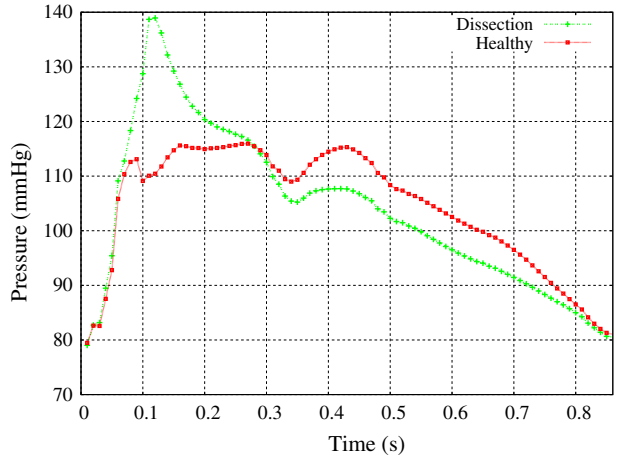

Figure 14. Comparison of inlet pressure history in healthy and dissected aortic arch.

Figure 12 shows the flow history of the second cardiac cycle of the 5th iteration in the dissected model. For comparison with the healthy case, both flow histories are superimposed in the graphs. During systole the flow deviates more to the uprising arteries, in comparison to the systolic phase of the healthy model. The excess of blood is compensated during diastole, during 300–400 ms, with the reverse flow values of the uprising outlets of the dissected model (refer to the autoregulation description in Section). This occurs because the uprising outlets are relatively closer to the geometrical abnormality, i.e. the dissection. Figure 13 shows the velocity vectors at peak systole. The dissected wall deviates the most the flow in the high velocity period of the cardiac cycle. The inlet, narrowed by the dissected wall, works as a nozzle, guiding the flow with a relatively high velocity to the uprising outlets. On the other hand, outlet 4 receives less blood during systole, with the shortage being compensated during diastole.

It is also of interest to compare the inlet pressure histories in the healthy and dissected aorta. Apart from the dissection effect on the flow history patterns, the obstacle causes a considerable increase in pressure at the aortic root, which in turn may affect the heart's blood ejection capacity. Figure 14 depicts the comparison of inlet pressure histories at the healthy aortic root and the corresponding graph in the dissected one. Figure 15 displays the pressure contours when the inlet pressure reaches its maximum value (0.11 s of cardiac cycle). The calculation indicates a 21% increase in the inlet peak pressure, which is a considerable value in terms of clinical diagnostics. The detection of an increase in inlet pressures may indicate the formation of an obstacle or disorder such as dissection, atheroma plaque, etc. Among the negative effects of sustained high pressures in the ascending aorta, heart hypertrophy and its excessive work can be mentioned. The higher pressures at aortic root require the heart to increase its pumping pressure to respond to the pressure and flow demands of the arterial system. Also, high arterial pressures may cause aneurysm or arterial ruptures at aortic root. In addition, a higher arterial wall stress as a result of a rise in blood pressure may increase the concentration of Low-Density Lipoproteins in arterial walls (Khanafer & Berguer 2009). On the other hand, at distal zones of the disorder, the autoregulation mechanism remains active to ensure that the blood demands are satisfied and this is a negative point for the nutrition of distal members: as the nutrition process follows the osmosis rule, due to permanent lower pressure difference between the artery and the organ (as a result of the autoregulation), the nutrients pass slower through the arterial walls.

3.3. Limitations

Although not being an objective of the present work, the pressure pulse transmission cannot be captured from the simulations in which the A+IPBC methodology is applied. Based on the proposed modified explicit FSI coupling strategy, the velocity of the solid domain is not transferred to the fluid domain, the parameter which is necessary for the calculation of pressure pulse transmission.

If the objective of a simulation is to study the local velocities of the fluid domain near to the FSI interface, the modified explicit FSI method is not capable to provide a precise velocity field as it is affected directly by the solid wall velocity, the parameter which is neglected in the proposed FSI scheme.

And finally, it can be emphasised that the explicit coupling is relatively faster in calculations but, at the same time, less precise than its implicit alternative. It must be added that the lower precision are negligible from clinical application point of view, which is the main objective of the A+IPBC methodology.

4. Conclusions

Based on the results presented and discussed in the previous section, the following conclusions can be offered:

- A new methodology has been proposed as an improved alternative to the conventional pressure-imposed boundary conditions. The methodology combines the autoregulation and impedance concepts in an in-house code to calculate the pressure histories that should be imposed at outlets of a CFD or FSI simulation. The calculations are fast and hence of particular interest for clinical and pre-surgery decisions.
- Neglecting the wall velocities during the data exchange between the solid and fluid domains, together with autoregulation, avoid the numerical instabilities or unrealistic results produced with conventional pressure-imposed and explicit FSI methodologies.
- Decoupling the solution of impedance equations from CFD computations accelerates the simulation process by reducing the computational costs, while the impedance concept is still incorporated in the analysis.
- The numerical simulations presented reproduce and allow studying the physiological phenomena; excessive or insufficient blood flows at the branches are compensated during systolic or diastolic phase of the cardiac cycle by the autoregulation mechanism.
- Numerical simulations show that the dissection in the ascending aorta causes an increase in the aortic root pressure, which can be a clinical indicator for detecting this disorder. This excess of blood pressure may not be measurable at distal cardiovascular sites, but hypertrophy may provide a signal in primary clinical checks.
- The heart movement and interaction with the arterial walls is incorporated in the simulations. This makes the analyses more realistic, but has little effect on the flow-split calculations. However, it does affect the results of the wall stress calculations. The same applies when spring elements are used to represent the surrounding arteries and tissues at outlets.

Disclosure statement

No potential conflict of interest was reported by the authors.

Acknowledgements

The authors acknowledge the funding received from the Spanish Ministry of Science and Innovation through the research project DPI2011-27609/DPI and are grateful to Dr Javier Rodríguez and other members of the staff of PRINCIPIA Ingenieros Consultores S.A. for their comments and collaboration.

References

Afkari D, Gabaldón F, Rodríguez J. 2014. Comparison of implicit and explicit FSI coupling strategies in cardiovascular system. In IV Reunión del Capítulo Español de la Sociedad Europea de Biomecánica (ESB); 20--21 November; Valencia, Spain.

Artoli A, Hoekstra A, Sloot P. 2006. Mesoscopic simulations of systolic flow in the human abdominal aorta. J Biomech. 39: 873–884.

Avolio AP. 1980. Multi-branched model of the human arterial system. Med Biol Eng Comput. 18: 709–718.

Bailevs Y, Gohean JR, Hughes TJR, Moseer RD, Zhang Y. 2009. Patient-specific isogeometric fluid-structure interaction analysis of thoracic aortic blood flow due to implantation of the jarvik 2000 left ventricular assist device. Comput Methods Appl Mech Eng. 198: 3534–3550.

Beller CJ, Labrosse MR, Thubrikar MJ, Szabo G, Robicsek F, Hagl S. 2005. Increased aortic wall stress in aortic insufficiency: clinical data and computer model. Eur J. Cardio-thoracic Surg. 27: 270–275.

Borghi A, Wooda N, Mohiaddinb R, Xua X. 2008. Fluid-solid interaction simulation of flow and stress pattern in thoracoabdominal aneurysms: A patient-specific study. J Fluids Struct. 24: 270–280.

Brezzi F, Fortin M. 1991. Mixed and hybrid finite element methods. Vol. 15, Springer series in computational mathematics. New York (NY): Springer.

Brezzi F, Lipnikov K, Shashkov M. 2005. New discretization methodology for diffusion problems on polyhedral meshes. T-7, MS B284. Theoretical Division, Los Alamos National Laboratory.

Brown AG, Shi Y, Marzo A, Staicu C, Valverde I, Beerbaum P, Lawford PV, Hose DR. 2012. Accuracy vs. computational time: Translating aortic simulations to the clinic. J Biomech. 45: 516–523.

Burman E, Fernández MA. 2009. Stabilization of explicit coupling in fluid-structure interaction involving fluid incompressibility. Comput Meth Appl Mech Eng. 198: 766–784.

Calvo FJ, 2006. Simulación del fluido sanguíneo y su interacción con la pared arterial mediante modelos de elementos finitos [Simulation of blood flow and its interaction with arterial wall using finite element methods] [doctoral thesis]. UPM: Madrid.

CD-adapco. 2012. Cd-adapco, star-ccm+. Melville, (NY): CD-adapco.

Demiray H. 1972. On the elasticity of soft biological tissues. J Biomech. 5: 241–311.

Figueroa CA, Baek S, Taylor CA, Humphrey JD. 2009. A computational framework for fluid-solid-growth modeling in cardiovascular simulations. Comput Methods Appl Mech Eng. 198: 3583–3602.

Figueroa CA, Taylor CA, Chiou AJ, Yeh V, Zarins CK. 2009. Magnitude and direction of pulsatile displacement forces acting on thoracic aortic endografts. J Endovascular Therapy. 16:350–358.

Gao F, Watanabe M, Matsuzawa T. 2009. Fluid-structure interaction within 3-layered aortic arch model under pulsatile blood flow. In Proceedings of the Sixth International Conference on Parallel and Distributed Computing, Applications and Technologies (PDCAT05); Computer Society. Dalian, China.

García-Herrera C. 2008. Comportamiento mecánico de la aorta ascendente: Caracterización experimental y simulación Numérica [Mechanical behaviour of ascending aorta: experimental characterization and numerical simulation] [doctoral thesis]. España: Departamento de Mecánica de Medios Continuos y Teoría de Estructuras, ETSI Caminos, Canales y Puertos, Universidad Politécnica de Madrid.

Gerbeau J-F, Vidrascu M, Frey P. 2005. Fluid-structure interaction in blood flows on geometries based on medical imaging. Comput Struct. 83: 155–165.

Huang RF, Yang T-F, Lan Y-K. 2010. Pulsatile flows and wall-shear stresses in models simulating normal and stenosed aortic arches. Exp Fluids. 48: 497–508.

Khanafer K, Berguer R. 2009. Fluid structure interaction analysis of turbulent pulsatile flow within a layered aortic wall as related to aortic dissection. J Biomech. 42: 2642–2648.

Kilner P, Yang G, Mohiaddin R, Firmin D, Longmore D. 1993. Helical and retrograde secondary flow patterns in the aortic arch studied by three-directional magnetic resonance velocity mapping. Circulation J Am Heart Assoc. 88: 2235–2247.

Kim H, Figueroa C, Hughes T, Jansen K, Taylor C. 2009. Augmented Lagrangian method for constraining the shape of velocity profiles at outlet boundaries for three-dimensional finite element simulations of blood flow. Comput Methods Appl Mech Eng. 198: 3551–3566.

Kim H, Vignon-Clementel I, Figueroa C, LaDisa J, Jansen K, Feinstein J, Taylor C. 2009. On coupling a lumped parameter heart model and a three-dimensional finite element aorta model. Ann Biomed Eng. 37:2153–2169.

Klipstein RH, Firmin DN, Underwood SR, Rees RS, Longmore DB. 1987. Blood flow patterns in the human aorta studied by magnetic resonance. British Heart J. 58: 316–323.

Les AS, Shadden SC, Figueroa CA, Park JM, Tedesco MM, Herfkens RJ, Dalman RL, Taylor CA. 2010. Quantification of hemodynamics in abdominal aortic aneurysms during rest and exercise using magnetic resonance imaging and computational fluid dynamics. Ann Biomed Eng. 38: 1288–1313.

Malvé M, del Palomar AP, Chandra S, López-Villalobos J, Mena A, Finol EA, Ginel A, Doblaré M. 2001. FSI analysis of a healthy and a stenotic human trachea under impedance-based boundary conditions. J Biomech Eng. 133.

Malvé M, García A, Ohayon J, Martínez M. 2012. Unsteady blood flow and mass transfer of a human left coronary artery bifurcation: FSI vs. CFD. Int Commun Heat Mass Transfer. 39: 745–751.

Mazzaro L, Almasi SJ, Shandas R, Seals DR, Gates PE. 2005. Aortic input impedance increases with age in healthy men and women. J Am Heart Assoc Hypertens. 45:1101–1106.

Milnor WR. 1975. Arterial impedance as ventricular afterload. Circulation Res J Am Heart Assoc. 36: 565–570.

Moireau P, Xiao N, Astorino M, Figueroa C, Chapelle D, Taylor C, Gerbeau J-F. 2011. External tissue support and fluid-structure simulation in blood flows. Biomech Model Mechanobiol. 11: 1–18.

Murgo J, Westerhof N, Giolma J, Altobelli S. 1980. Aortic input impedance in normal man: relationship to pressure wave forms. Criculation J Am Heart Assoc. 62: 105–116.

Nicholas WW, O'Rourke MF. 2005. McDonald's blood flow in arteriess. 5th ed. Hodder Arnold. London. ISBN:0340809418/0-340-80941-8.

Olufsen MS. 1998. Modeling the arterial system with reference to an anesthesia simulator [doctoral thesis]. Denmark: Department of Mathematics, Roskilde University.

O'Rourke MF, Taylor MG. 1967. Input impedance of the systemic circulation. Criculation Res J Am Heart Assoc. 20:365–380.

Papaharilaou Y, Ekaterinaris JA, Manousaki E, Katsamouris AN. 2007. A decoupled fluid structure approach for estimating wall stress in abdominal aortic aneurysms. J Biomech. 40: 367–377.

Polindara C, Blanco S. Goicolea J. 2013. Nuevos desarrollos en la caracterización geométrica y determinación de índices de ruptura de las paredes arteriales. CMN2013; Bilbao, Spain.

Qiao A, Liu Y. 2008. Medical application oriented blood flow simulation. Clin Biomech. 23: S130–S136.

Scotti CM, Cornejo SL, Finol EA. 2007. Biomechanics of abdominal aortic aneurysms: flow-induced wall stress distribution. ICCES. 1: 41–47.

Shahcheraghi N, Dwyer HA, Cheer AY, Barakat AI, Rutaganira T. 2002. Unsteady and three-dimensional simulation of blood flow in the human aortic arch. J Biomech Eng. 124: 516–523.

Sharp MK, Pantalos GM, Minich L, Tani LY, McGough EC, Hawkins JA. 2000. Aortic input impedance in infants and children. J Appl Physiol. 88: 2227–2239.

SIMULIA. 2014. Abaqus users' manual v6.14. SIMULIA.

Suo J. 2005. Investigation of blood flow patterns and hemodynamics in the human ascending aorta and major trunks of right and left coronary arteries using magnetic resonance imaging and computational fluid dynamics [doctoral thesis]. School of Biomedical Engineering, Georgia Institute of Technology, Atlanda.

Tan F, Borghi A, Mohiaddin R, Wooda N, Thom S, Xu X. 2009. Analysis of flow patterns in a patient-specific thoracic aortic aneurysm model. Comput Struct. 87: 680–690.

Taylor CA, Hughes TJR, Zarins CK. 1998. Finite element modeling of three-dimensional pulsatile flow in the abdominal aorta: relevance to atherosclerosis. Ann Biomed Eng. 26: 975–987.

Urquiza S, Blanco P, Vénere M, Feijóo R. 2006. Multidimensional modelling for the carotid artery blood flow. Comput Methods Appl Mech Eng. 195: 4002–4017.

Vignon-Clementel IE. 2006. A coupled multidomain method for computational modeling of blood flow [doctoral thesis]. CA: Mechanical Engineering Department, Stanford University. Stanford, California.

Vignon-Clementel IE, Figueroa CA, Jansen KE, Taylor CA. 2010. Outflow boundary conditions for 3d simulations of non-periodic blood flow and pressure fields in deformable arteriess. Comput Methods Biomech Biomed Eng. 13: 1–16.

Vlachopoulos C, O'Rourke M. 2000a. Current problems in cardiology. Medical Professional Unit. Sydney: St. Vincent's Hospital, U. New South Wales.

Vlachopoulos C, O'Rourke M. 2000b. Current problems in cardiology, genesis of the normal and abnormal arterial pulse. Sydney: Mosby, University of New South Wales.

Votta E, Guiducci L, Morbiducci U, Redaelli A. 2008. Numerical sensitivity analysis of mechanical factors triggering aortic arch tearing. J Biomech. 16th ESB Congress Oral Presentation. Volume 41, Supplement 1, Page S39.

Zhao S, Xu X, Hughes A, Thom S, Stanton A, Ariff B, Long Q. 2000. Blood flow and vessel mechanics in a physiologically realistic model of a human carotid arterial bifurcation. J Biomech. 33: 975–984.